https://doi.org/10.20965/ijat.2014.p0903

Paper:

Development of a Non-Rigid Micro-Scale Cutting Mechanism Measuring the Cutting Force Using an Optical Lever

German Herrera-Granados*, Kiwamu Ashida, Ichiro Ogura**, Yuichi Okazaki**, Noboru Morita*, Hirofumi Hidai*, Souta Matsusaka*, and Akira Chiba***

*Graduate School of Engineering, Chiba University
1-33 Yayoi-cho, Inage-ku, Chiba-shi, Chiba 263-8522, Japan
E-mail: german.hg@chiba-u.jp
**AMRI, National Institute of Advanced Industrial Science and Technology (AIST)
1-2-1 Namiki, Tsukuba-shi, Ibaraki 305-8564, Japan
E-mail: ashida.k@aist.go,jp
[Received April 17, 2014; accepted July 25, 2014]

A new cutting mechanism for the fabrication of micro-scale grooves is presented in this study. Based on the control principle of the nano-cutting mechanism using an Atomic Force Microscope (AFM), in the newly developed system, a single crystal diamond tool is mounted at the free edge of a cantilever beam and is used for the removal of material. During the cutting process, the cantilever undergoes a deformation that is required for the implementation of a machining force feedback control. It was experimentally observed that the use of this mechanism enables to maintain the cutting depth of the micro-grooves constant even if they are fabricated on inclined surfaces; this is achieved by maintaining the normal cutting force constant using a feedback controller. For this experimental system, an optical lever is used to measure the angular deformation at the tip of the cantilever, thus providing a better understanding of total cutting force involved in the machining process.

Keywords: micro-cutting, constant cutting force, optical lever, AFM machining, v-groove

1. Introduction

Recently, the fabrication of micro-textured surfaces has been in great demand in various industrial fields owing to its numerous applications. More specifically, the fabrication of micro-grooves is one of the most important features in mechanical, electronics, photonics and biomedical applications, such as for the development of micro lens arrays, micro-channels for heat exchangers, and micro/mesa arrays for biomedical devices [1].

Several micro-machining technologies are available for the development of such micro-textured surfaces, e.g., Micro-Electro-Discharge Machining (MEDM), lithography electroforming molding (LIGA), laser machining and ElectroChemical Machining (ECM). However most of these technologies have several disadvantages related to the limitations of the material properties or the cost involved in each manufacturing process [2].

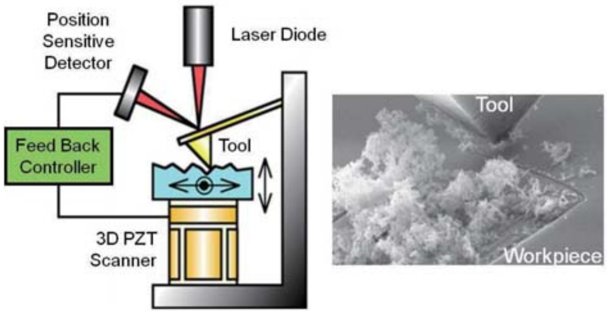

Fig. 1. Nano-cutting mechanism using AFM.

On the other hand, ultra-precision machining using diamond tools is being increasingly applied in the fabrication of high-precision machined parts for advanced industrial applications. The extremely high hardness and crystalline structure of diamond enable the fabrication of diamond cutters with very sharp cutting edges that are necessary for ultra-precision machining [3]. Some techniques that employ diamond tools have been developed for the fabrication of micro-grooves [1, 2, 4–8]; however, the main disadvantage of such techniques resides in the fact that the precision of the machine needs very strict control, because any error in the motion mechanism (thermal deformations, geometrical deviations, etc.) will be transferred directly to the machined work.

A new cutting technique for the fabrication of micro-grooves that is based on the control principle of the nano-cutting mechanism using an Atomic Force Microscope (AFM) [9–18] (**Fig. 1**) was proposed in previous works [19–21]. In this cutting mechanism, micro-grooves are formed using a cantilever with a commercial diamond tool chip attached to its free edge, and that under a sufficiently high normal load it is possible to remove material. To maintain the cutting depth constant, a displacement sensor, piezoelectric actuator (PZT) and Force Feed-

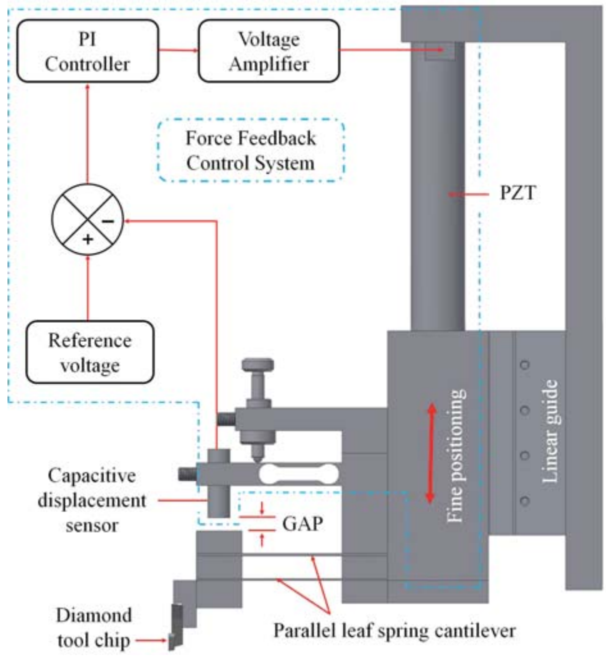

Fig. 2. Schematic of the previously developed cutting mechanism.

Back Controller (FFBC) are used to control the relative displacement between the tool tip and the material surface, which consequently gives a constant normal cutting force.

The ability of this cutting mechanism to maintain the normal force constant during different cutting experiments realized on inclined surfaces has been demonstrated [21]. However, owing to its characteristics, this mechanism does not provide all the information required to understand the cutting process involved. For this reason, a new cutting mechanism using a different sensing method is presented in this study, which enables a deeper examination of the deformation of the cantilever for further investigation of the cutting process.

2. Parallel Leaf Spring Cantilever Mechanism Setup

The previously developed cutting mechanism, whose schematic is shown in **Fig. 2**, consists of a single crystal diamond tool chip that is mounted at the edge of a flexible parallel leaf spring cantilever. To control the normal cutting force, the relative position between the tool and the workpiece (GAP) is sensed during the entire process using a capacitive displacement sensor. The GAP value is compared with a reference voltage in the implemented Proportional-Integral (PI) controller; the resultant output is a signal that will be sent to a PZT, which will provide fine position displacement in order to maintain constant the deformation of the cantilever and hence, the normal cutting force. The displacement sensor, the PI controller and the PZT constitute the FFBC, which is also shown in

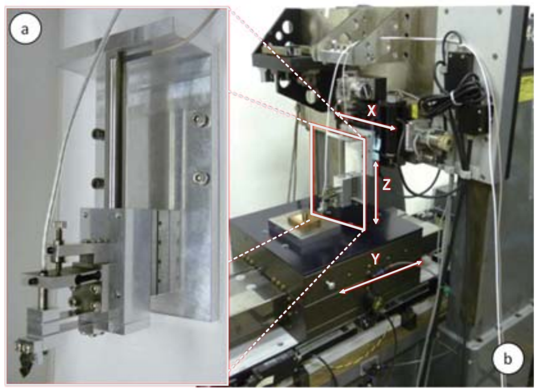

Fig. 3. Previously developed experimental system a) Cutting mechanism, b) three-axis machine tool.

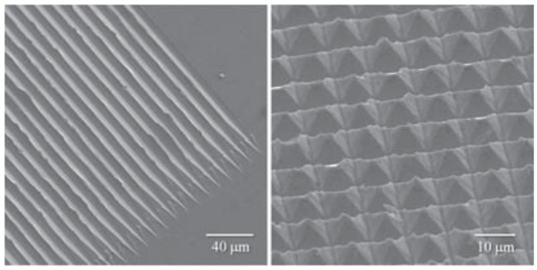

Fig. 4. Different groove arrays fabricated using previously developed cutting mechanism.

Fig. 2 [21].

To achieve a larger manufacturing area, the cutting mechanism is mounted on a three-axis Numerical Control (NC) machine tool, as shown in **Fig. 3**. One advantage of this system is that the FFBC can compensate part of the geometrical errors of the machine tool used. By this mechanism, V-grooves with cutting depths of up to 50 μm and lengths in the order of centimeters can be fabricated in a single cutting. Linear arrays of grooves can be realized in one or two directions, thereby permitting the fabrication of simple micro-structures such as pyramidal arrays (**Fig. 4**).

As mention previously, cutting experiments were performed in [21] to observe the behavior of this mechanism. When the FFBC is active, the system maintains the cutting depth of the grooves constant even if the machining is performed on an inclined surface. **Fig. 5** shows a schematic of a cutting experiment performed on inclined surfaces, as well as the normal cutting force recorded during this experiment. The graph shows the variation of the normal cutting force (vertical axis) while the tool displaces along the cutting axis (horizontal axis). **Fig. 6** shows Scanning Electron Microscope (SEM) images that compare the micro- grooves fabricated when the FFBC was active with those when it was not active. It is observed that the width of the groove (w_G) – which is directly related to the cutting depth (d_G) and the cutting angle of the tool (θ_T) by the Eq. (1) – increases as the tool displaces along the cutting axis when the FFBC is not active.

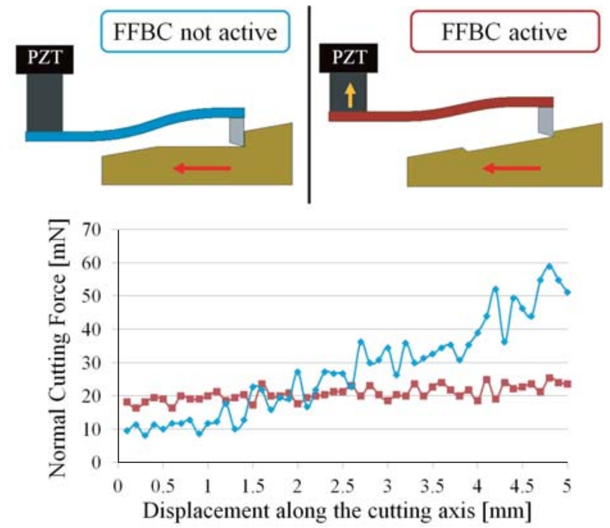

Fig. 5. Cutting experiments on inclined surfaces.

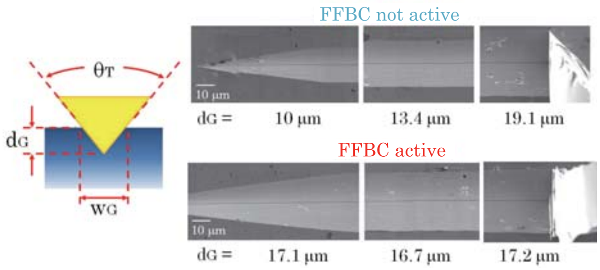

Fig. 6. Micro-grooves fabricated on an inclined surface.

However, when the FFBC is active, the cutting depth is maintained constant during the machining process.

After observing the behavior of this mechanism during several cutting experiments, some drawbacks were detected. For the cutting experiments, the total cutting force (F_T) is considered to have a normal component (F_N) and a horizontal component (F_H) as shown in **Fig. 7**. However, owing to the characteristics of the sensor used, only the normal component can be estimated using Hooke's law for springs (Eq. (2)), where the F_N denotes the normal cutting force, δ is the deformation of the cantilever (GAP), and the k is the cantilever stiffness, which is 37.1 mN/μm for this mechanism.

$$d_G = \frac{w_G}{2 \cdot \tan\left(\frac{\theta_T}{2}\right)} \quad \ldots \ldots \ldots \ldots \quad (1)$$

$$F_N = k \cdot \delta \quad \ldots \ldots \ldots \ldots \ldots \ldots \quad (2)$$

A parallel leaf spring cantilever was implemented to obtain a linear deformation on the cantilever during the cutting process, which was measured by the capacitive sensor. However, through Finite Element Analysis (FEA) (**Fig. 8**), it was observed that the deformation of the cantilever is affected by the cutting direction, and a non- linear deformation was observed. To observe the impact of the cutting direction on the cantilever deformation, cutting experiments were performed in forward and backward directions; the obtained results are shown in **Fig. 9**, where the normal cutting force (vertical axis) is plotted as function of the cutting depth of the groove (horizontal axis). The results confirm that the cutting direction affects the behavior of the cantilever, but owing to the characteristics of the capacitive sensor, it is not possible to describe how its deformation occurs.

A new cutting mechanism was proposed to estimate the total cutting force components (F_N and F_H) (**Fig. 7**), by simultaneously measure the torsional and flexural deformation of the cantilever with an optical lever. The proposed system is also expected to provide additional information about the cutting process.

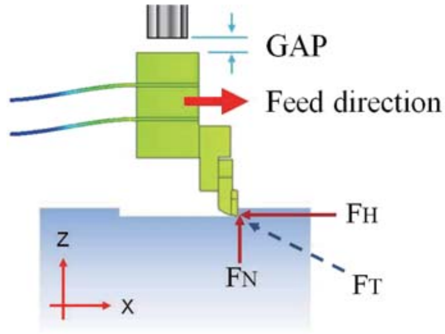

Fig. 7. Cutting forces in micro-groove fabrication process.

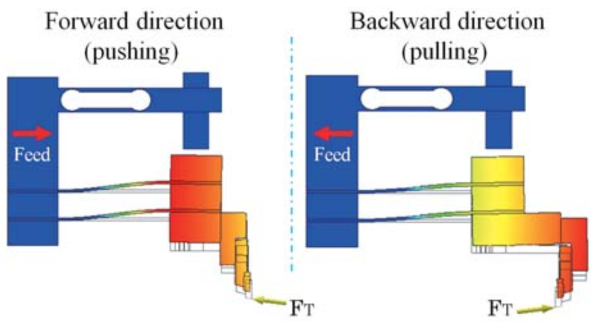

Fig. 8. Effect of cutting direction on the cantilever deformation using FEA.

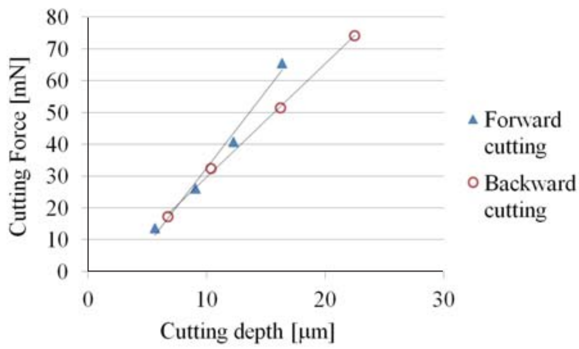

Fig. 9. Results of cutting experiments in forward and backward directions.

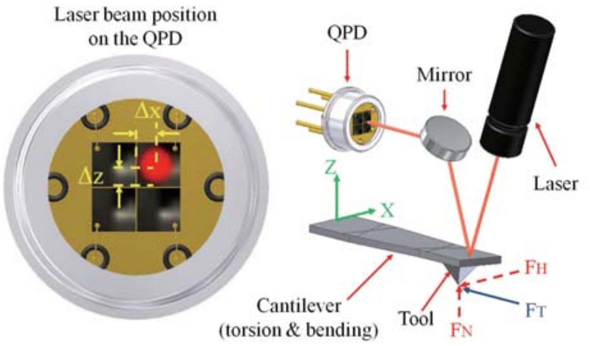

Fig. 10. Concept of the newly proposed sensing method.

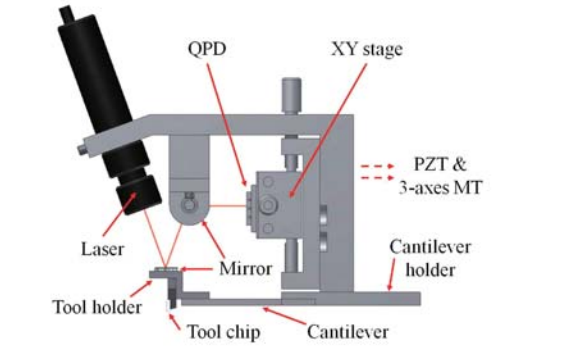

Fig. 11. Schematic of newly proposed cutting mechanism.

3. Single Leaf Spring Cantilever Mechanism Setup

The proposed optical lever consists of a Quadrant PhotoDiode (QPD) as the detector, a laser as the light source, and an array of mirrors to direct the laser beam to the measurement point (**Fig. 10**).

According to **Fig. 10**, to apply the flexural and the torsional deformations to the cantilever beam, the cutting will have to be performed perpendicular to its larger axis; then, the horizontal cutting force (F_H) will be obtained by the torsion at the free edge of the cantilever, measured by the displacement Δx on the QPD, whereas the vertical or normal cutting force (F_N) will be obtained by its flexion, measured by the displacement Δz on the QPD.

Both cutting mechanisms have similar dimensions, because of which they can be adapted indistinctly to the PZT actuator as well as to the motion mechanism. A single cantilever beam is mounted because the optical lever measures the angular deformation of the cantilever instead of the linear displacement, as is necessary for the capacitive sensor. Because of this change, the fabrication of cantilever beams with different geometrical characteristics such as length, thickness and shape is proposed, in order to observe the impact of the cantilever stiffness on the cutting process. The position of the tip of the diamond tool remains the same for all the cantilever beams, even if the cutting will be performed in different directions (forward, backward and lateral). Two mirrors – one at the free edge of the cantilever beam and the other in the body of the mechanism – are mounted to direct the laser beam from the light source to the QPD. To set the initial incidence position of the laser beam on the QPD, the QPD is mounted on an XY-stage. **Fig. 11** shows a schematic of the newly proposed cutting mechanism, whereas **Fig. 12** shows the overall system.

A more detailed calibration of this mechanism has been presented in [22]; a summary of this calibration is shown in **Fig. 13**, from which it can be seen that the sensitivity and stiffness of the cantilever beam change depending on its geometrical characteristics. The shape (rectangular or trapezoidal), thickness T, and length L depend on the cantilever selected. For rectangular cantilevers, the width W is kept constant at 10 mm, whereas

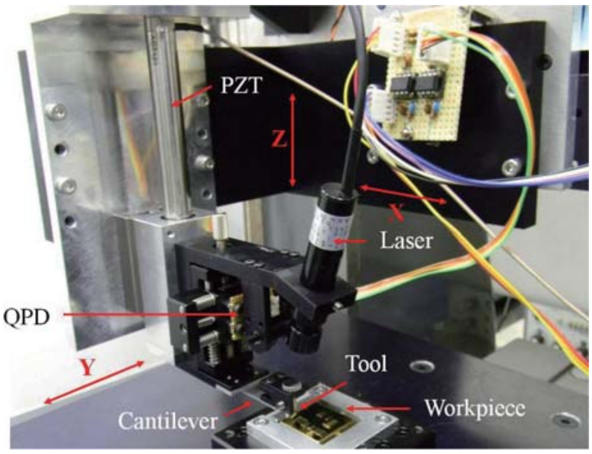

Fig. 12. Newly proposed mechanism with optical lever.

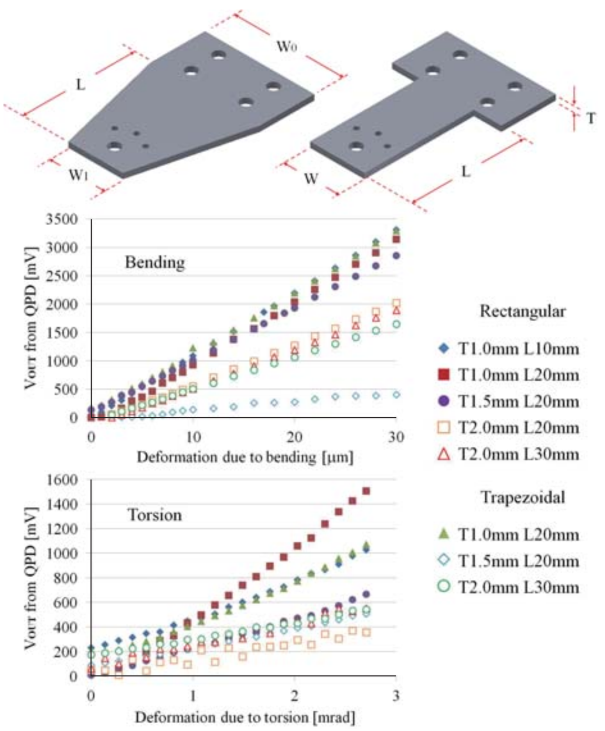

Fig. 13. Sensitivity of cantilevers with different geometries.

Table 1. Conditions of cutting experiments with the new cutting mechanism.

Material	Brass
Inclination	$<+3/10000$
Cutting length	3 mm
Cutting depth	5, 10, 15, 20 μm
Feed rate	6 mm/min
Cutting type	Dry and orthogonal cutting
Tool	Single crystal diamond tool
Cutting angle	90°
Cutting direction	Forward, backward and lateral
Cantilever	Rectangular, L 10 mm T 1.0 mm

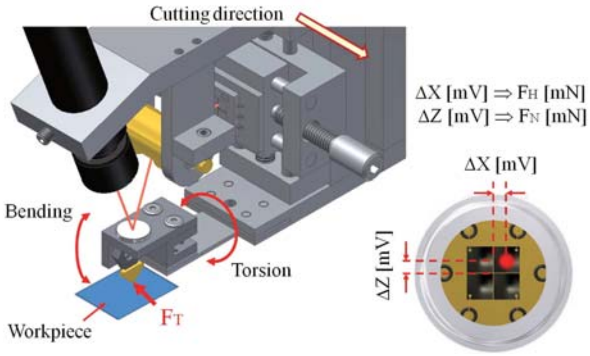

Fig. 14. Schematic of the lateral cutting.

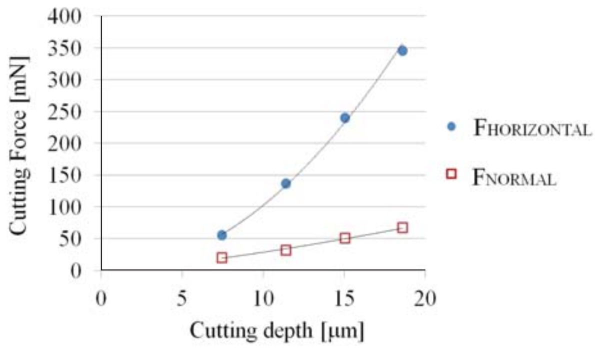

Fig. 15. Cutting force components during lateral cutting.

for trapezoidal cantilevers, the longer (W_0) and shorter (W_1) sides are 20 and 10 mm, respectively. The results presented in this paper are obtained from cutting experiments performed with a cantilever with a thickness of 1 mm, and a length of 20 mm. Under bending, this cantilever exhibits a sensitivity 110.4 mV/μm and rigidity of 17.9 mN/μm. In contrast, under torsion, its sensitivity is approximately 592.5 mV/mrad and its torsional constant is 2042.3 mN·mm/mrad.

4. Cutting Experiments

Several cutting experiments were done to evaluate the performance of the new cutting mechanism. The cutting conditions of these experiments are presented on **Table 1**. For these experiments the FFBC was not active.

When the cutting is performed in the forward and backward directions, it is not possible to determine the total cutting force (F_T), because only the vertical component (F_N) can be measured. However, when the experiments are performed in the lateral direction, both components of the total cutting force (F_N and F_H) can be determined using the output voltage from the QPD and the calibration performed previously (**Fig. 14**). **Fig. 15** shows a plot of the normal cutting force F_N and horizontal cutting force F_H as function of the cutting depth of the groove. The results show that F_H accounts approximately 80% of the total force, which is a common value in mechanical cutting.

To verify the accuracy of the measured cutting force, the experimental results were compared with theoretical calculations for the deformation on the cantilever. From [23–24] and considering **Fig. 10** as reference, it can be observed that the Hooke's law for cantilevers (Eq. (3)) can be used to estimate the deformation on the cantilever by employing its geometrical properties. In this equation, the vector Δ denotes the cantilever tip's deflection, the tensor C is the inverse stiffness tensor, and the F is the force vector. For simplicity, Eq. (3) can be rewritten as Eq. (4), considering that deformations on the cantilever beam other than its torsion and bending can be ignored because they are very small.

$$\Delta = C^{-1}F \quad \text{(3)}$$

$$\begin{bmatrix} \Delta x \\ \Delta z \end{bmatrix} = \begin{bmatrix} c_{xx} & 0 \\ 0 & c_{zz} \end{bmatrix} \begin{bmatrix} Fx \\ Fz \end{bmatrix} \quad \text{(4)}$$

From the general Euler-Bernoulli beam bending equation, it is possible to determine the constant c_{zz} as shown in Eqs. (5) – (7). Here, it is important to mention that Eqs. (6) – (8) are valid only for cantilever beams with a rectangular transverse area. In these equations, l, w and t denote the length, width and thickness, respectively, of the cantilever; E is the Young's modulus of the cantilever's material; and J_z is the moment of inertia,

$$\Delta z = \frac{l^3}{3EJ_z}Fz \quad \text{(5)}$$

$$J_z = \frac{wt^3}{12} \quad \text{(6)}$$

$$\Delta z = \frac{4l^3}{Ewt^3}Fz \quad \text{(7)}$$

$$c_{zz} = \frac{4l^3}{Ewt^3} \quad \text{(8)}$$

The constant c_{zz} is the largest coefficient of the tensor C and will appear as part of other coefficients.

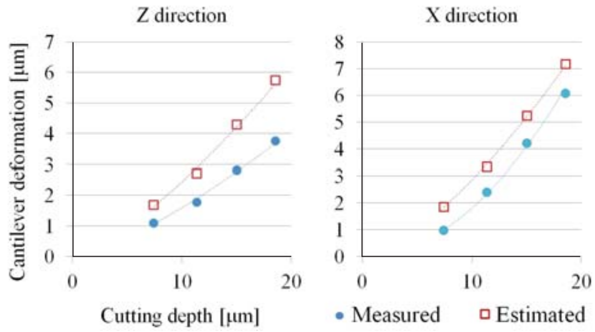

Fig. 16. Actual and estimated cantilever deformations.

The component of the cutting force in the X direction will induce torsion and bending to the cantilever beam. Eqs. (9) – (12) are derived from [23]. Here, l_{tip} denotes the distance between the tool tip and the cantilever beam. Finally, Eq. (13) is derived to estimate the deformation of the cantilever beam in the X and Z directions. **Fig. 16** shows a comparison of the theoretical and experimental results. To evaluate the equations, the experimental cutting force is used to calculate the cantilever deformation, which is then compared with the deformation measured by the optical lever.

$$\Delta x = \Delta x_{bend} + \Delta x_{tors} = (c_{bend} + c_{tors})Fx \quad \text{(9)}$$

$$c_{bend} = \frac{4l^3}{Ew^3t} \quad \text{(10)}$$

$$c_{tors} = \frac{8l_{tip}^2 l}{Ew^3t} \quad \text{(11)}$$

$$c_{xx} = \left(\frac{2l_{tip}^2}{l^2} + \frac{t^2}{w^2}\right) \cdot c_{zz} \quad \text{(12)}$$

$$\begin{bmatrix} \Delta x \\ \Delta z \end{bmatrix} = c_{zz} \cdot \begin{bmatrix} \left(\frac{2l_{tip}^2}{l^2} + \frac{t^2}{w^2}\right) & 0 \\ 0 & 1 \end{bmatrix} \begin{bmatrix} Fx \\ Fz \end{bmatrix} \quad \text{(13)}$$

From **Fig. 16**, it is found that the experimental and theoretical results are in agreement, thus verifying the validity of the information obtained from the measurement system.

Finally, cutting experiments were also performed in the forward, backward, and lateral directions in order to observe the capability of the new sensing system to show the deformation of the cantilever depending on the cutting direction. In this case, only the data required to calculate the normal cutting force can be obtained from the QPD output. A summary of the results obtained from the three experiments is shown in **Fig. 17**.

The figure shows that the cutting forces measured during the three experiments were significantly different even though the experiments were performed under the same cutting conditions. An important point to note is that negative values of the cutting force were observed during cutting in the forward direction. For the forward and the backward cutting processes, the deformations of the cantilever during indentation were very similar; however, when the mechanism started moving along the cutting axis, the edge of the cantilever showed a different deformation, as shown in the schematic in **Fig. 18**.

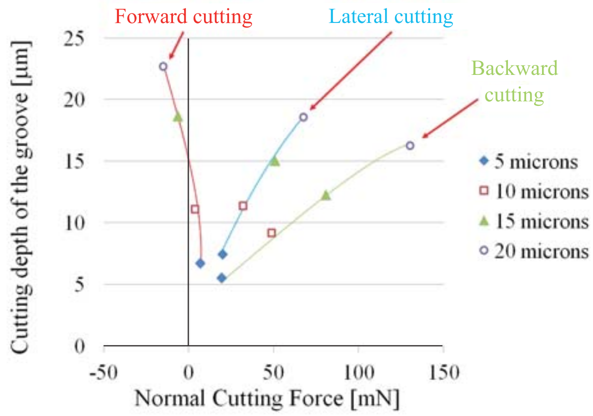

Fig. 17. Plot of normal cutting force versus cutting depth of groove for three different cutting directions.

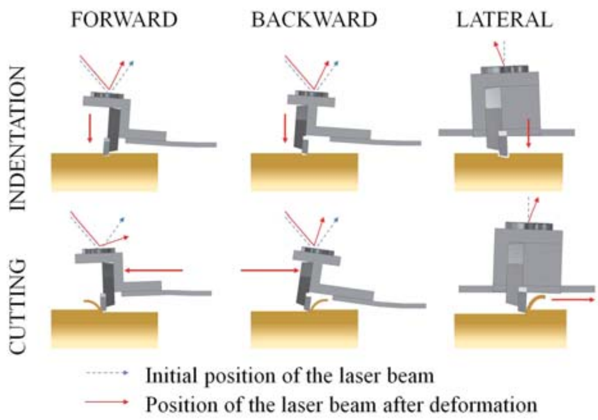

Fig. 18. Deformation of cantilever for three different cutting directions.

In the case of backward cutting, the deformation of the cantilever was observed to occur in the same direction as that by the indentation process because the diamond tool was pulled against the workpiece surface; this means that the larger the cutting depth, the larger is the output voltage obtained from the QPD. However, when the experiment is performed in the forward direction, the mechanism pushes the tool against the material surface, inducing an abnormal deformation at the edge of the cantilever (contrary to the deformation due to the indentation process). As result, in forward cutting, when the cutting depth is increased, the abnormal deformation is larger, and therefore, the output recorded at the QPD can have negative values. It is important to point that in both cases (forward and backward cutting), the normal (F_N) and the horizontal (F_H) components of the cutting force contributes in the

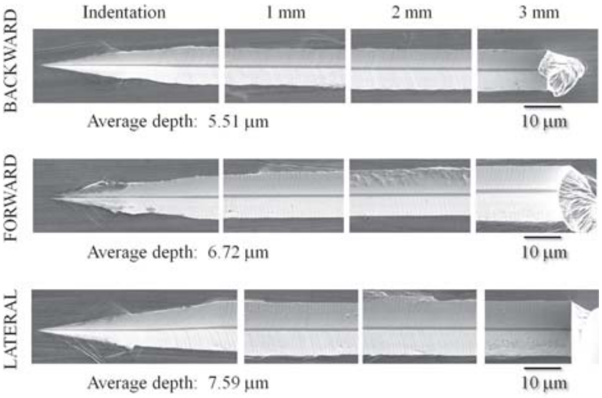

Fig. 19. Scanning Electron Microscope (SEM) images of the micro-grooves fabricated under three different cutting directions.

bending of the cantilever beam. In the case of lateral cutting, the flexural deformation of the cantilever beam has a similar behavior to that during backward cutting, but smaller in magnitude. This is because in the lateral cutting process, the horizontal component F_H, which is the largest component of the cutting force, produces torsion on the cantilever, whereas the normal component F_N generates the flexural deformation.

Figure 19 shows SEM images of micro-grooves with an initial indentation of 5 μm. In these images, it can be observed that the actual cutting depth is different from the indentation depth. This is because, as explained in **Fig. 18**, after the indentation process, the cantilever undergoes a different deformation depending on the cutting direction. Specifically, in the case of forward cutting, the cutting depth increases when the tool is running along the cutting axis, because the tool is being pushed into the material. In the cases of the lateral and backward cutting, however, the cutting depth remains constant during the process.

It is important to consider that the tool is mounted on a non-rigid mechanism, and therefore vibration occurs at the edge of the cantilever, especially when the cutting depth is too large. In order to reduce the vibration during the manufacturing of large grooves, and subsequently to improve the quality of the machined surface, it is recommended that cantilever beams with larger stiffness should be used and cutting should be performed in layers, where several passes are required to achieve a specific cutting depth.

5. Summary

A non-rigid cutting mechanism that uses a control principle similar to that of the nano-cutting experiment using an AFM mechanism has been developed.

In previous stages of this research, it was demonstrated that the fabrication of micro-grooves with a constant cutting depth, even on inclined surfaces, is possible by using a Force FeedBack Controller (FFBC). However, the sensor used for the FFBC is capable of detecting only linear displacements, making it difficult to completely understand the cutting phenomenon involved in this experiment.

To overcome this inconvenience, a new cutting mechanism that employs an optical lever as the sensing method was proposed to obtain more information about the cutting forces involved in the manufacturing process. To evaluate the performance of this new mechanism, several cutting experiments were performed, obtaining as result the following conclusions.

a) When the experiment is performed in the lateral direction (cutting axis is orthogonal to the longest side of the cantilever), it is possible to measure the total cutting force by measuring the flexural and torsional deformations of the cantilever beam used.

b) It was observed experimentally that the horizontal component of the cutting force accounts approximately for 80% of the total cutting force, which is a common value for mechanical cutting.

c) To determine the accuracy of the cutting force measured by the mechanism, a theoretical analysis based on the geometrical characteristics of the cantilever beam was done. The experimental and theoretical results demonstrated that the force measured by the mechanism is a good approximation of the actual cutting force. However, for future experiments, implementation of force sensor is recommended to verify the experimental results.

d) The difference between the results of cutting experiments performed in different directions (backward, forward, and lateral) was analyzed. Given the abnormal deformation observed in forward cutting, the use of backward or lateral cutting is recommended, with the lateral cutting providing additional advantage.

e) Because the tool was mounted on a non-rigid mechanism, vibration was observed to occur during the cutting experiments. For this reason, it is recommended that grooves should be fabricated by sequential layers, especially when the cutting depth is large. Another advantage of this new mechanism is the possibility of use different kinds of cantilever beams, each with a different stiffness. Surface quality and tool life are two parameters that should be considered in future experiments.

f) The actual cutting depth differs from the initial cutting indentation, set by the motion system. This phenomenon is directly related to the deformation of the cantilever beam, depending on the cutting direction. This parameter should therefore be calibrated in order to compare the cutting forces in each case more accurately.

Acknowledgements

This study was supported by the Japan Society for the Promotion of Science KAKENHI Grant Number 26289022. Its support is gratefully acknowledged.

References:

[1] F. Z. Fang, et al., "Fabrication of Micro Grooves," ASPE, 18th annual meeting, 2003, Portland, USA.

[2] G. D. Kim, et al., "Characteristics of chip formation in micro V-grooving using elliptical vibration cutting," J. Micromech. Microeng., Vol.17, pp. 1458-1466, 2007.

[3] A. Q. Biddut, et al., "Performance of single crystal diamond tools with different rakes angles during micro-grooving on electroless nickel plated die materials," Int. J. Adv. Manuf. Tech., Vol.33, Issues 9-10, pp. 891-899, 2007.

[4] D. Dornfeld, et al., "Recent Advances in Mechanical Micromachining," Annals of the CIRP, Vol.55, pp. 745-768, 2006.

[5] X. Ding, et al., "Ultra-precision cutting of micro-channels on Ni-copper: Effects on diamond cutter wear and workpiece surface finish," SIMTech technical report, Vol.10, pp. 209-215, 2009.

[6] T. Moriya, et al., "Creation of V-shaped microgrooves with flat-ends by 6-axis control ultraprecision machining," CIRP – Manufacturing Technology, Vol.59, pp. 61-66, 2010.

[7] G. D. Kim., et al., "Machining of micro-channels and pyramid patterns using elliptical vibration cutting," Int. J. Adv. Manuf. Technology, Vol.49, pp. 961-968, 2010.

[8] J. M. Lee, et al., "Micro grooving simulation and optimization in the roughing stage," Int. J. of Precision Eng. and Manuf., Vol.11, No.3, pp. 361-368, 2010.

[9] K. Ashida, et al., "Study on Nano-Machining Process Using Mechanism of a Friction Force Microscope," JSME Int. J., Series C, Vol.44, No.1, pp. 244-253, 2001.

[10] N. Kawasegi, et al., "Nanomachining of Silicon Surface Using Atomic Force Microscope With Diamond Tip," J. Manuf. Sci. Eng., Vol.128, Issue 3, pp. 723-729, 2006.

[11] Y. D. Yan, et al., "Investigation on AFM-based micro/ nano-CNC machining system," Int. J. of Machine tools & Manufacture, Vol.47, pp. 1651-1659, 2007.

[12] J. Shimuzu, et al., "Mold Pattern Fabrication by Nanoscratching," Int. J. Automation Tech., Vol.7, No.6, pp. 686-693, 2013.

[13] Y. D. Yan, et al., "3D force components measurement in AFM scratching tests," J. Ultramicroscopy, Vol.105, pp. 62-71, 2005.

[14] W. Gao, et al., "Experiments using a Nano-machining Instrument for Nano-Cutting Brittle Materials," CIRP, Vol.49, Issue 1, pp. 439-442, 2000.

[15] J. C. Huang, et al., "A study of nanomachining and nanopatterning on different materials using atomic force microscopy," Int. J. of Materials and Product Technology, Vol.49, No.1, pp. 57-71, 2014.

[16] Y. Geng, "Fabrication of millimeter scale nanochannels using the AFM tip-based nanomachining method," Applied Surface Science, Vol.266, pp. 386-394, 2013.

[17] J. C. Huang, et al., "The study of nanoscratch and nanomachining on hard multilayer thin films using atomic force microscope," Scanning, Vol.34, Issue 1, pp. 51-59, 2012.

[18] Y. Yan, et al., "Top-Down Nanomechanical Machining of Three-Dimensional Nanostructures by Atomic Force Microscopy," Small, Vol.6, Issue 6, pp. 724-728, 2010.

[19] K. Ashida, et al., "Basic study of micro-groove cutting using a elastic leaf spring type tool holder," Int. Conf. on MicroManufacturing, 2011, Tokyo, Japan.

[20] G. Herrera-Granados, et al., "Micro-groove cutting for different materials using an elastic leaf spring type tool holder," Key Engineering Materials, Vols.523-524, pp. 93-98, 2012.

[21] G. Herrera-Granados, et al., "Basic study on micro/nano scale cutting applying machining force control system," JSPE, Spring meeting, 2013, Tokyo, Japan.

[22] G. Herrera-Granados, et al., "Development of a micro/nano-scale constant load cutting mechanism measuring the cutting force by an optical lever," Int. Conf. on LEM21, 2013, Miyagi, Japan.

[23] Technical notes, www.ntmdt.jp/data/media/files/spm_basics/cantilever.pdf [accessed on October 15, 2014]

[24] L. Kumanchik, et al., "Simultaneous normal and torsional force measurement by cantilever surface contour analysis," Measurement Science and Technology, Vol.22, No.5, 055103, 2011.

Name:
German Herrera-Granados

Affiliation:
Doctor Student, Graduate School of Engineering, Chiba University

Address:
1-33 Yayoi-cho, Inage-ku, Chiba-shi, Chiba 263-8522, Japan

Brief Biographical History:
2007- Center of Applied Sciences and Technological Development, UNAM
2010- Technical training at AIST, Japan
2012- Doctor Student at Chiba University, Japan

Membership in Academic Societies:
- Japan Society for Precision Engineering (JSPE)
- Japan Society of Mechanical Engineers (JSME)

Name:
Kiwamu Ashida

Affiliation:
Senior Researcher, AMRI, National Institute of Advanced Industrial Science and Technology (AIST)

Address:
1-2-1 Namiki, Tsukuba-shi, Ibaraki 305-8564, Japan

Brief Biographical History:
2001- Chief Government Officer at Ministry of Economy, Trade and Industry
2002- National Institute of Advanced Industrial Science and Technology
2008- Visiting Researcher at VTT Technical Research Centre, Finland

Membership in Academic Societies:
- Japan Society of Mechanical Engineers (JSME)
- Japan Society for Precision Engineering (JSPE)

Name:
Ichiro Ogura

Affiliation:
Researcher, AMRI, National Institute of Advanced Industrial Science and Technology (AIST)

Address:
1-2-1 Namiki, Tsukuba-shi, Ibaraki 305-8564, Japan

Brief Biographical History:
1999- Mechanical Engineering Laboratory (MEL), AIST
2004- New Energy and Industrial Technology Development Organization (NEDO)
2006- National Institute of Advanced Industrial Science and Technology

Membership in Academic Societies:
- Japan Society for Precision Engineering (JSPE)
- American Society for Precision Engineering (ASPE)

Name:
Yuichi Okazaki

Affiliation:
Senior Researcher, AMRI, National Institute of Advanced Industrial Science and Technology (AIST)

Address:
1-2-1 Namiki, Tsukuba-shi, Ibaraki 305-8564, Japan

Brief Biographical History:
1979- Mechanical Engineering Laboratory (MEL), AIST
1991- Visiting Researcher at IPT-FhG, Germany
2001- National Institute of Advanced Industrial Science and Technology

Membership in Academic Societies:
- Japan Society for Precision Engineering (JSPE)
- American Society for Precision Engineering (ASPE)

Name:
Souta Matsusaka

Affiliation:
Assistant Professor, Department of Mechanical Engineering, Chiba University

Address:
1-33 Yayoi-cho, Inage-ku, Chiba-shi, Chiba 263-8522, Japan

Brief Biographical History:
1999- Joining and Welding Research Institute, Osaka University
2001- Department of Mechanical Engineering, Chiba University

Membership in Academic Societies:
- Japan Society for Precision Engineering (JSPE)
- Japan Society for Abrasive Technology (JSAT)
- Japan Welding Society (JWS)

Name:
Noboru Morita

Affiliation:
Professor, Department of Mechanical Engineering, Chiba University

Address:
1-33 Yayoi-cho, Inage-ku, Chiba-shi, Chiba 263-8522, Japan

Brief Biographical History:
1983- Toshiba Corp
2002- Professor at Toyama University
2011- Professor at Chiba University

Membership in Academic Societies:
- Japan Society for Precision Engineering (JSPE)
- Japan Society for Abrasive Technology (JSAT)

Name:
Akira Chiba

Affiliation:
Staff, Department of Mechanical Engineering, Chiba University

Address:
1-33 Yayoi-cho, Inage-ku, Chiba-shi, Chiba 263-8522, Japan

Brief Biographical History:
1983- Mitsubishi Electric Corp.
2003- Renesas Electronics Corp.
2013- Chiba University

Membership in Academic Societies:
- Japan Society for Precision Engineering (JSPE)
- Japan Society for Abrasive Technology (JSAT)

Name:
Hirofumi Hidai

Affiliation:
Associate Professor, Department of Mechanical Engineering, Chiba University

Address:
1-33 Yayoi-cho, Inage-ku, Chiba-shi, Chiba 263-8522, Japan

Brief Biographical History:
1999- Assistant Professor at Tokyo Institute of Technology
2010- Associate Professor at Chiba University

Membership in Academic Societies:
- Japan Society for Precision Engineering (JSPE)
- Japan Society for Abrasive Technology (JSAT)
- Japan Society of Laser Technology (JSLT)